processes

MDPI

Article

A Dynamic Simulation of a Piezoelectric Energy-Harvesting System Integrated with a Closed-Loop Voltage Source Converter for Sustainable Power Generation

Ahmed K. Ali [1,*], Ali Abdulwahhab Abdulrazzaq [2] and Ali H. Mohsin [3]

[1] Institute of Technology, Middle Technical University, Baghdad 10074, Iraq
[2] Technical Instructors Training Institute, Middle Technical University, Baghdad 10074, Iraq; dr.ali.abdulwahhab@mtu.edu.iq
[3] Air Conditioning and Refrigeration Techniques Engineering Department, College of Engineering and Technologies, Al-Mustaqbal University, Babylon 51001, Iraq; ali.hasanain.mohsin@uomus.edu.iq
* Correspondence: engineer28ahmed@gmail.com or ahmed_khalid@mtu.edu.iq

Abstract: Numerous recent studies address the concept of energy harvesting from natural wind excitation vibration to piezoelectric surfaces, aerodynamic losses, and electromagnetic dampers. All these techniques require a connection to an energy-management circuit. However, the simulation model for energy conversion and management dedicated to this task has not yet been described. This paper presents a model-based simulation for an energy conversion system using piezoelectric energy-harvester system (PEHS) technology. A controlled pulse width modulation (PWM) rectifier, a closed-loop buck-boost converter, and a piezoelectric transducer comprise a dynamic mathematical model of a PEHS. The control blocks of the closed-loop buck-boost converter use the perturbation and observation (P&O) algorithm based on maximum power point tracking (MPPT), which adapts the operational voltage of the piezoelectric source to deliver the maximum power to load. A simulation program is employed to perform mathematical analysis on various wind vibration scenarios, piezoelectric sources without PWM converters, and piezoelectric vibration sources connected to a closed-loop P&O converter. The crucial results of this paper demonstrated that the proposed dynamic PEHS model effectively fed low-power electronic loads by directly adjusting the output voltage level to the set voltage, even under different vibration severity levels. As a result, the proposed PEHS dynamic model serves as a guideline for researchers in the development of self-powered sensors, which contributes to understanding sustainable energy alternatives.

Keywords: controlled PWM rectifier; P&O MPPT; closed-loop converter; piezoelectric energy harvesting; sustainable renewable energy

check for updates

Citation: Ali, A.K.; Abdulrazzaq, A.A.; Mohsin, A.H. A Dynamic Simulation of a Piezoelectric Energy-Harvesting System Integrated with a Closed-Loop Voltage Source Converter for Sustainable Power Generation. *Processes* **2024**, *12*, 2198. https://doi.org/10.3390/pr12102198

Academic Editors: Federica Raganati and Hsin-Jang Shieh

Received: 19 August 2024
Revised: 13 September 2024
Accepted: 30 September 2024
Published: 10 October 2024

Copyright: © 2024 by the authors. Licensee MDPI, Basel, Switzerland. This article is an open access article distributed under the terms and conditions of the Creative Commons Attribution (CC BY) license (https://creativecommons.org/licenses/by/4.0/).

1. Introduction

Daily activities and production processes frequently demonstrate inefficiencies in energy use, resulting in the inadequate harnessing of significant amounts of energy and its release into the atmosphere as various forms of waste heat. This event results in substantial waste and environmental degradation. Since the initial observation of piezoelectric electricity (PE), extensive research efforts have been dedicated to exploring its diverse applications [1–5]. On the other hand, wind-induced vibrations offer a valuable source of potential for electrical power generation [6]. The vibrational force is used as input to generate AC electricity that changes sinusoidally, which is further rectified to be practical for power applications [7]. The outline of the state-of-the-art in power-management circuits for PEHS was reported in [8]. It covered various power-management techniques for different PEHS circuits. In the same context, the current work contributes to integrating these techniques with a new control strategy using dynamic simulation to improve PEHS performance.

Ericka et al. [9] presented an approach for energy harvesting with a circular piezoelectric membrane to optimize energy production derived from mechanical vibrations. Their system has a significantly improved conception of piezoelectric materials and geometric arrangements, laying the groundwork for more efficient energy-harvesting devices.

Wang et al. [10] focused on the enhancement of energy-harvesting systems using a piezoelectric circular diaphragm array. This array structure improved energy production and efficiency, making it possible to collect vibration energy on a larger scale and making piezoelectric harvesters more useful. Barton et al. [11] studied energy harvesting with a nonlinear oscillator, tackling the constraints of linear systems in low-frequency and wideband vibrations. Using nonlinear dynamics, they improved the energy-harvesting efficiency in fluctuating conditions, advancing more versatile and functional energy systems. Mitcheson et al. [12] explored the adjustment of resonance frequency and damping in electromagnetic energy harvesters using power electronic circuits.

Wu et al. [13] introduced a piezoelectric energy harvester that adjusts its resonance frequency in response to wind speed fluctuations. This technique enhances the offshore wind-energy-gathering efficiency by dynamically adapting to fluctuating cases, marking a significant advancement in optimizing energy conversion in changeable conditions. Meng et al. [14] conducted a study that provided significant insights into the effectiveness of various geometric designs via a comparative analysis of two geometric spheres and cylinder shapes for piezoelectric energy-harvester devices.

Wang et al. [15] conducted an experimental and analytical investigation to study the design of a nonlinear sickle-shaped cantilever beam piezoelectric energy harvester for wind energy applications. Their study enhanced the design of piezoelectric energy harvesters by demonstrating the efficacy of nonlinear geometric shapes in optimizing energy conversion. Kan et al. [16] developed a new axially retractable bracket-shaped piezoelectric vibrator that uses magnetic force for wind energy harvesting. They discussed a practical application of magnetic stimulation to enhance the vibrational responsiveness of piezoelectric materials. The suggested design presents an innovative method for enhancing the energy-harvesting efficiency by integrating piezoelectric material technologies and voltage control circuits.

Zhao et al. [17] described the combination of two approaches involving a nanogenerator on the sole of a shoe to use energy from walking. They presented a new device architecture that combines flexible thermoelectric and piezoelectric materials to increase the overall power output while reducing the effect on shoe functionality. Additionally, Wang et al. [18] presented an innovative electrical power generation device that uses high-frequency dynamic piezoelectric deformation through shear caused by friction. Despite these advances, research initiatives concentrating on power generation via piezoelectric and thermal means remain relatively limited. Various mechanisms have been used to increase the efficiency of smart tiles, including wearable biomechanical energy harvesting, triboelectric pairs, and mechanical impact mechanisms. Krishnasamy et al. [19] proposed the conversion of the input vibration force, which is dependent on the vibration frequency, as a common method for harvesting piezoelectric energy.

Yingyong et al. [20] presented a system that uses piezoelectric cantilevers (PZCs) connected to the moving surface of a tile to generate alternative electricity. The principle of the presented system comes from the human footstep, because people walking by can produce a mechanical impact, which generates kinetic energy. To maintain frequency movement, a fixed mass is placed at the end of the PZCs. Panthongsy et al. [21] suggested an approach using the principle of a magnetic tension mechanism to increase vibration in PZCs. In this configuration, a permeant magnet attached to one end and an iron piece fastened to the moving surface of the tile act as activators for the piezoelectric consoles. When individuals step on the tile, the moving surface descends, reducing the distance between the iron piece and the permeant magnet, thus causing attraction. On the basis of the passage, the tile surface returns to its original position, separating the magnet from the iron piece and inducing vibration in the piezoelectric console. In the same context, many mechanical methods have been used to harness the energy of smart tiles, although with

considerable friction. Duarte et al. [22] presented the rack-and-pinion mechanical approach, in which the gear connected to the moving surface of the tile interacts with a pinion gear connected to a generator. With tile stimulation, gear rotation drives the gear pinion, thereby activating the generator to produce energy. In this instance, the applied force directly stimulates the piezoelectric cells, facilitating energy production. The study presented by Puscasu et al. [23] adopted a similar approach by placing PE cells beneath the tile surface, using pedestrian-induced force to drive energy production. Their findings emphasized the capacity of piezoelectric flooring as a sustainable solution for urban lighting, especially in regions with significant pedestrian activity. Building on this, Kim et al. [24] investigated the utilization of the triboelectric effect within a tile structure and explored the dielectric effects to improve energy harvesting. The electromagnetic effect uses coils around the perimeter of the tile and a central disc that holds magnets. The disc rotates due to the applied force, which creates flux on the coils [25,26].

In a deeper delve into the field, Balato et al. [27] explored techniques in resonant piezoelectric vibration energy harvesters (RPVEHs). These devices generate electrical power from vibrating sources, but their optimal operating point changes over time as input vibrations vary. This study focuses on the most common RPVEH architecture, which employs a diode bridge rectifier and a DC/DC converter. Additionally, it provides experimentally validated guidelines for parameter selection in two popular maximum power point tracking (MPPT) techniques (perturb and observe and open-circuit voltage). The simulation results are analyzed to assess the efficacy of the proposed modeling method. A previous study [28] explored the modeling of a piezoelectric bender to convert ambient vibrations into electrical energy. It compared an analytical approach based on beam theory with two existing models. Lefeuvre et al. [29] delved into a design buck-boost converter for sensor-less power optimization in PEHS. Their proposed buck-boost converter circuit improved the energy extraction efficiency of piezoelectric materials without the need for an external feedback sensor. This sensor-less power-management approach proved effective in improving PEHS performance, particularly in situations where vibration sources were inconsistent. Although they addressed a crucial issue in converter design, their discussion remains limited as they solely concentrated on energy extraction without guaranteeing stability in the produced power. Building on this, Mitcheson et al. [30] introduced a different approach for controlling the resonant frequency and damping of energy harvesters using power electronics circuits. While their focus was on frequency tuning, the current research incorporates this aspect while placing a strong emphasis on enhancing piezoelectric efficiency, developing electromechanical models, and optimizing the rectification-conversion process.

In PEHSs, converter circuits play a critical role in the management of usable power. Cai and Zhu [31] delved into improving the performance of electromagnetic harvesters by developing the converter circuit with microcontrollers. Their integration approach is similar to the current study, but the process of converting the vibration energy source to usable power is different. The wind force is still an unstable source of vibrational energy. Cai et al. [32] highlighted the importance of bistable processes and nonlinear energy sinks for better energy collection from wind-induced vibrations, particularly in offshore areas where conditions are harsh and changeable. Although Cai et al. concentrated on optimizing the structure using bistable energy sinks, the current study adopts a systems approach by designing a simulation model that converts vibrational force into a reliable electrical output, appropriate for many applications. The combination of PE with advanced power electronics represents a distinct but equally groundbreaking advancement in the realm of energy harvesting. To the best of our knowledge, the current study makes novel contributions by presenting a new dynamic simulation model using wind-induced vibrations with piezoelectric materials, an area that has not been thoroughly explored in previous literature [17–28].

Previous studies have proposed many useful models for PE energy harvesting, but few of them have concentrated on investigating the dynamic simulation of these models.

However, this paper delves into the theoretical modeling of PE vibration energy harvesting and the associated DC–DC boost converter. The aim of this paper is to present a new approach to the use of wind-induced vibrations for energy harvesting by developing a detailed dynamic simulation model. The simulation analysis focuses on achieving a constant DC output of the energy harvested. The following is a summary of the key contributions:

- An approach to harnessing the energy vibrations caused by wind, which can be harnessed as a source of electrical power, is explored. More precisely, we present a comprehensive and detailed dynamic mathematical model for a PEHS that combines a piezoelectric transducer, a regulated PWM rectifier, and a closed-loop buck-boost converter. This model accurately depicts the intricate correlation between wind-induced mechanical vibrations and the subsequent conversion of electrical energy, offering a more precise portrayal of real-life conditions.
- This paper emphasizes the efficiency of PEHS in response to vibrations, which makes them suitable for energy-harvesting performance across a spectrum of low and high vibration frequencies.
- An electromechanical dynamic simulation model is developed to represent the piezoelectric materials harvester, which translates the vibrational force into the electrical output. The process entails converting the vibration of the piezoelectric sheet sinusoidally, varying AC output into rectified DC output suitable for power applications. This approach broadens the current understanding of the dynamic simulation and mathematical representation of PEHS across various excitation frequencies, both high and low. It consolidates the simulations of vibration originating from diverse wind energy sources, such as those generated by cars passing on a highway.
- The piezoelectric model is also interconnected with an electrical circuit that has a PWM single-phase bridge rectifier and a DC–DC boost converter that is controlled by a P&O MPPT to obtain greater stability in power output.

2. Piezoelectric Harvester Model

The electromechanical model diagram for a piezoelectric-based energy harvester consists of many components and primarily incorporates wind vibrations. Figure 1 depicts the functional schematic of a wind vibration energy harvester that utilizes piezoelectric technology.

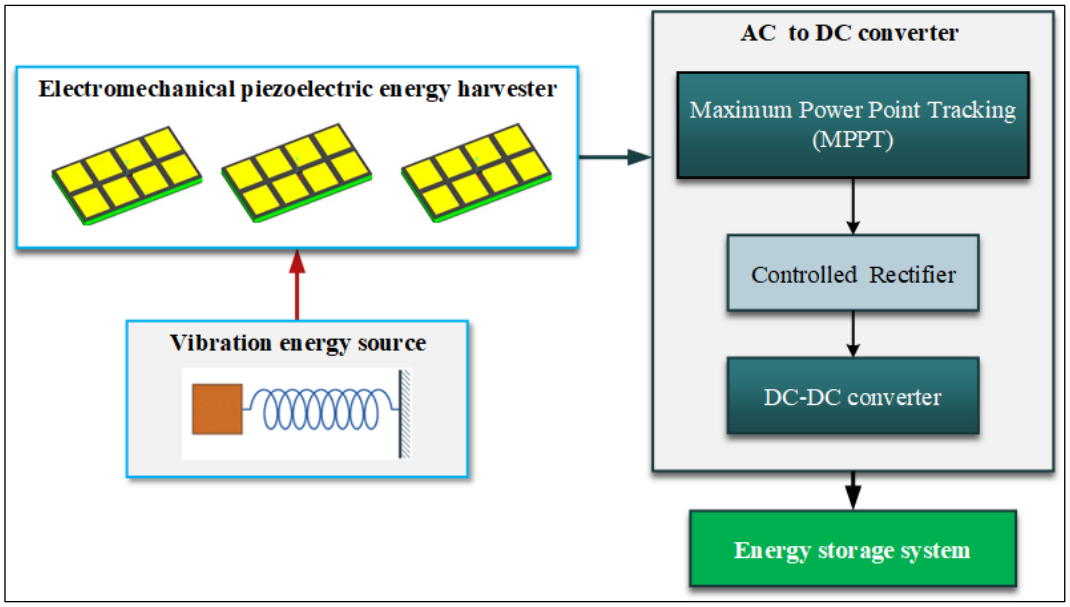

Figure 1. Diagram of the piezoelectric energy harvester for wind-generated vibrations.

1. Vibration source: Wind can cause vibrations in a structure. This structure can be a cantilever beam or any other resonant structure specifically built to oscillate due to wind-induced vibrations [33].
2. Piezoelectric materials: The direct piezoelectric effect converts mechanical strain into a train of electrical charges [34].
3. Electrical output: The piezoelectric material generates an electrical charge, which it immediately collects, stores, or uses as electrical power.
4. Energy storage management: This circuit divides a group of capacitors or batteries into rectifiers, voltage regulators, a DC-to-DC converter, and possibly an energy storage device [7].

A piezoelectric transducer converts mechanical vibrations from a wind force into an oscillating train of electrical charges. The sinewave peak-to-peak level relationship describes the changeable values of these charges, which depend on the severity of the wind vibration [35]. The controlled PWM rectifier, in conjunction with a closed-loop buck-boost converter, converts this train of sinewave cycles into DC voltages.

The piezoelectric vibration energy harvester uses a complex second-order mass spring damper model to fully describe its dynamic behavior [28,36]. Within this model, the harvester frame is composed of a mass, denoted as M, suspended by a spring characterized by its stiffness constant, μ_k, and a damper with a coefficient μ_D. This damper embodies various sources of mechanical damping, such as wind-induced vibrations and air friction. The application of an external force to the system induces movement in the mass, which in turn causes deformation in the connected piezoelectric element.

The principle of the piezoelectric effect governs this idea by generating an electric voltage when mechanical stress is applied to the piezoelectric material.

Crucially, we assumed that the external vibrational force acting on the system follows a sinusoidal pattern [37]. Thus, variations in wind speed and direction that exert aerodynamic forces on the turbine structure can be assumed in a sinusoidal manner, and we can express this force mathematically, as follows:

$$F_{wind}(t) = F_0 \sin(\omega t + \theta) \tag{1}$$

where F_0 represents the amplitude of the force, ω is the angular frequency of the sinusoidal vibrational force, t denotes time, and θ is the angle between the direction of the wind and the direction of motion of the harvester frame. This equation concisely captures the sinusoidal nature of the external vibrational force, which in turn induces harmonic motion in the harvester frame, facilitating efficient energy harvesting [37]. The equation of motion in a second-order mass–spring damper system describes the relative motion of the mass with respect to the frame, represented as $x(t)$ [38]. When the influence of wind as an external force is considered, the equation becomes $F_{wind}(t)$, resulting in:

$$F_{wind}(t) = M\frac{d^2x(t)}{dt^2} + \mu_D\frac{dx(t)}{dx} + \mu_k x(t) \tag{2}$$

where $x(t)$ represents the displacement of the mass from its equilibrium position. The acceleration of the mass is $\frac{d^2x(t)}{dt^2}$. The velocity of the mass is $\frac{dx(t)}{dx}$.

In order to calculate the formal transfer function of the system, first it needs to express the equation of motion in terms of the Laplace transform and then solve for the output, $X(s)$, in terms of the input force, $F_{wind}(s)$. When all initial conditions are zero, the transfer function, $H(s)$, is defined as follows:

$$H(S) = \frac{1}{Ms^2 + \mu_D s + \mu_k} \tag{3}$$

In the case of nonzero initial conditions, the transfer function can be expressed as:

$$H(\mathrm{S}) = \frac{\mathrm{Ms}^2}{\mathrm{Ms}^2 + \mu_\mathrm{D}\mathrm{s} + \mu_\mathrm{k}} \tag{4}$$

The mass, M, and stiffness, μ_k, of the system define the natural frequency:

$$\omega_n = \sqrt{\frac{\mu_\mathrm{k}}{\mathrm{M}}} \tag{5}$$

where ω_n is the natural frequency, which represents the frequency at which a system oscillates in the absence of damping ($\mu_\mathrm{D} = 0$). The mass and stiffness of the system dictate its intrinsic attributes. The damping ratio, ζ, can be expressed in terms of the damping coefficient, μ_D, as:

$$\zeta = \frac{\mu_\mathrm{D}}{2\sqrt{\mathrm{M}}\mu_\mathrm{k}} \tag{6}$$

The damping ratio, ζ, reveals the rate at which oscillations diminish after the system is subjected to a disturbance. It compares actual damping, μ_D, with the critical damping, $2\sqrt{\mathrm{M}}\mu_\mathrm{k}$, which represents the lowest level of damping required to avoid oscillations.

3. Modeling Interfaced Electrical Circuits

This section explores the methodology of modeling interconnected electrical circuits, involving transfer functions, impedance analysis, and a state–space model, to predict the PEHS precisely.

3.1. PWM Full-Wave Rectifier

A power electronic circuit, known as a pulse width modulation (PWM) single-phase bridge rectifier, converts the AC voltage to the control DC voltage in the output voltage. The rectifier employs the PWM technique to regulate the output voltage. When the duty cycle of the PWM signal supply to the bridge switches is varied, the effective voltage of the load can be adjusted. The rectifier circuit typically uses MOSFETs or IGBTs as switches. To regulate the output voltage, the PWM signal controls these switches.

Figure 2 shows the principal circuit configuration of a single-phase voltage source PWM converter. The switches T_1 through T_4 are fully controllable. On the AC side, the inductance is denoted as L_m, where R_m represents the corresponding resistance. The DC side includes a filter capacitor labeled C_d. Furthermore, the terms U_s and i_s refer to the voltage and current of the AC supply, whereas U_ab and U_Dc indicate the voltage on the AC side and the output voltage on the DC side, respectively [39].

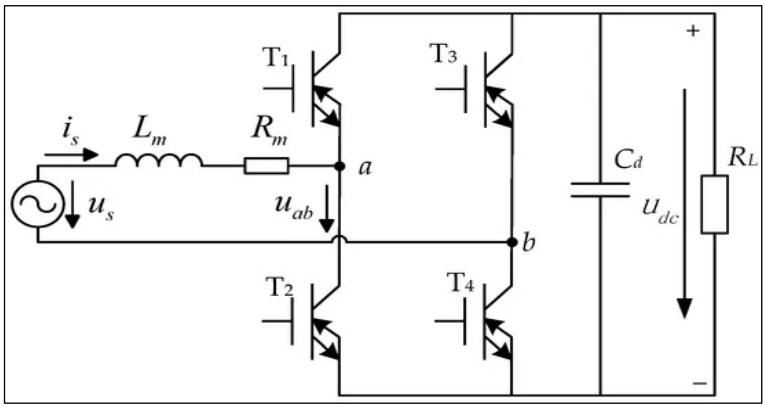

Figure 2. Essential circuit layout of a single-phase voltage source PWM converter featuring an RC-IGBT.

The rectifier employs PWM to regulate the operation status of four switches. Generally, the average output voltage over the bridge in a phase-controlled rectifier is often defined as:

$$\mathrm{U_{Phase-DC}} = \frac{U_{peak}}{\pi}(1 + \cos(\alpha)) \tag{7}$$

where $\mathrm{U_{Phase-DC}}$ is the phase-controlled rectifier output DC volage, U_{peak} is the peak of input AC voltage, and α represents the firing angle. The firing angle is used to control turn-on devices, such as thyristors (SCRs), in a fully controlled rectifier to determine when in the AC waveform the two complementary switches are turned on [40]. Thus, the output DC voltage in the phase-controlled rectifier is controlled by the firing angle, α, which achieved a maximum output voltage when $\alpha = 0^\circ$ and a minimum voltage when $\alpha = 180^\circ$.

Power electronics applications, such as DC–DC converters and PWM rectifiers, commonly use PWM-controlled circuits. The following formula provides the output voltage of a PWM-controlled converter [41]:

$$\begin{gathered} \mathrm{T_{off}U_{DC}} = \mathrm{T_sU_{in}} \\ D = \frac{\mathrm{T_{On}}}{\mathrm{T_s}} \end{gathered} \tag{8}$$

where $\mathrm{U_{in}}$ is the input voltage, and D represents the duty cycle of the PWM signal. A PWM converter controls the output voltage by varying the duty cycle of the PWM waveform. The duty cycle, D, is defined as the ratio of $\mathrm{T_{On}}$, which is the duration for which the PWM signal is on (high), to the sample time, $\mathrm{T_s}$, which is the total period of the PWM signal (sum of the on and off times). In this study, we proposed that the voltage-second equation depends on the $\mathrm{T_{On}}$, so it can be written as:

$$1/\mathrm{T_{on}U_{DC}} = \mathrm{T_sU_{in}} \tag{9}$$

The duty cycle typically ranges from 0 to 1, where 0 represents the PWM signal being fully off and where 1 represents the PWM signal being fully on. Adjusting the duty cycle between 0 and 1 allows fine control of the output voltage within this range [40]. In real-time scenarios, it is advisable to avoid a duty cycle of D = 1 since it may potentially result in an infinite DC voltage. However, the voltage across the DC load can be adjusted to meet the desired specifications by selecting an appropriate duty ratio [41]. In order to find the average DC voltage of the PWM rectifier for the main part of the vibration voltage, the fully controlled rectified voltage (Equation (7)) must be sub-stationed at a maximum output voltage, where $\alpha = 0^\circ$ with respect to the PWM switching into Equation (9). Therefore, the average DC output voltage of a single-phase PWM bridge rectifier can be expressed as:

$$\mathrm{U_{DC}} = \frac{2U_{max_{a-b}}}{\pi}\mathrm{D} \tag{10}$$

where $U_{max_{a-b}}$ represents the maximum amplitude of the vibration voltage. In the PWM rectifier, each PWM waveform has a D that determines the on/off duration of the corresponding switch, $\mathrm{T_1}$–$\mathrm{T_4}$. The duty cycles, D{$\mathrm{T_1}$–$\mathrm{T_4}$}, are typically adjusted to ensure that the output voltage is regulated [42].

3.2. DC–DC Converter

The DC–DC converter converts the DC input voltage source into either a step-up or a step-down of the DC output voltage. In piezoelectric vibrational energy-harvester applications, a buck-boost converter is a widely used type of DC-to-DC converter to regulate the output voltage. The operation mode increases or decreases depending on the duty cycle of the PWM signal. The typical buck-boost converter consists of an inductor, a power electronic switch, a diode, and a capacitor, as illustrated in Figure 3. Typically, a capacitor is placed across the output to reduce the voltage ripple and stabilize the output voltage. The control circuit, which is an important part of the buck-boost converter, includes a PWM

generator that is responsible for controlling the switches by generating a changeable duty cycle to control the switches. In a closed-loop system, the output voltage remains at a certain level on the basis of feedback from the output voltage [40].

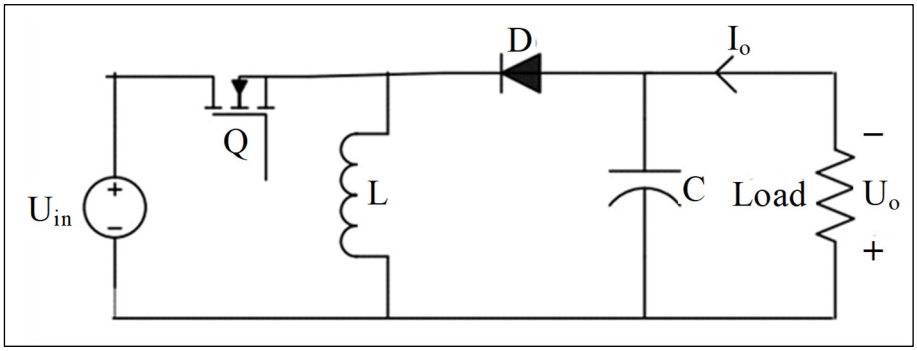

Figure 3. A traditional buck-boost converter circuit.

The expression for the output voltage of a buck-boost converter is defined as:

$$U_{B-DC} = \frac{D}{1-D} U_{DC} \tag{11}$$

where U_{B-DC} is the output voltage.

On the basis of the output voltage equation, the circuit controls the output voltage by regulating the duty cycle. Even in cases where the input voltage varies, the converter can regulate the output voltage by modifying the duty cycle.

3.3. Maximum Power Point Tracking (MPPT) Algorithm

The MPPT technique, which is based on perturbation and observation (P&O) algorithms, obtains the optimal output voltage and enhances the power transfer efficiency from the DC–DC converter to the load. The P&O MPPT technique typically determines whether the system operates at its maximum power point [27]. The P&O MPPT technique uses the rectified output voltage and output current signals to ascertain the operation point that can transfer the maximum power by adjusting the conversion output voltage. In this paper, the P&O MPPT aims to ensure that the energy-harvesting system operates at maximum power. The PWM generator block uses the signal from the P&O MPPT block to produce the reference duty cycle, allowing adaptable control for the DC–DC converter output voltages. The P&O MPPT algorithm consistently monitors the rectifier output voltage and current, even in the presence of varying wind vibration frequencies. Figure 4 illustrates the sequential operation of the MPPT technique, which is based on the P&O algorithm [43]. On the basis of the flowchart for the P&O MPPT algorithm, the duty cycle appears to play a crucial role in determining the energy transfer from the piezoelectric device to the load. By simultaneously adjusting the duty cycle via the P&O algorithm, the system ensures that it consistently operates at maximum energy conversion efficiency.

The implemented P&O MPPT block diagrams, which combine closed-loop control of a DC-to-DC converter, are shown in Figure 5. The implementation solely utilizes Simulink blocks—it does not incorporate scripting code. The flowchart of the P&O algorithm provides recommendations for marking each block with its role in the implanted P&O MPPT. The MPPT based on the P&O algorithm starts by accepting voltage and current readings from the rectifier outputs U_{DC} and I_{DC}, respectively.

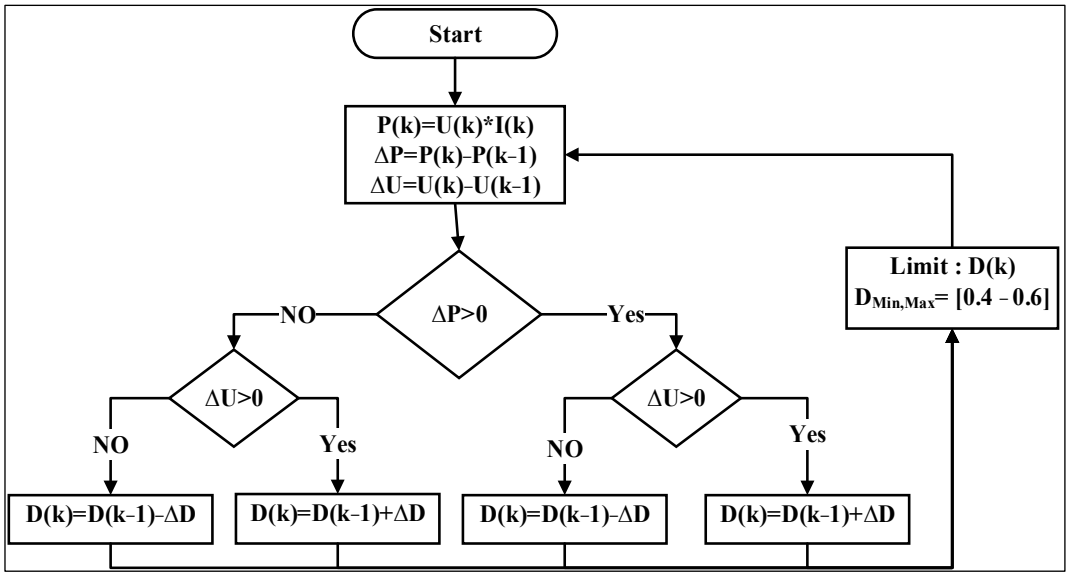

Figure 4. The flowchart of the perturb and observe (P&O) MPPT algorithm system.

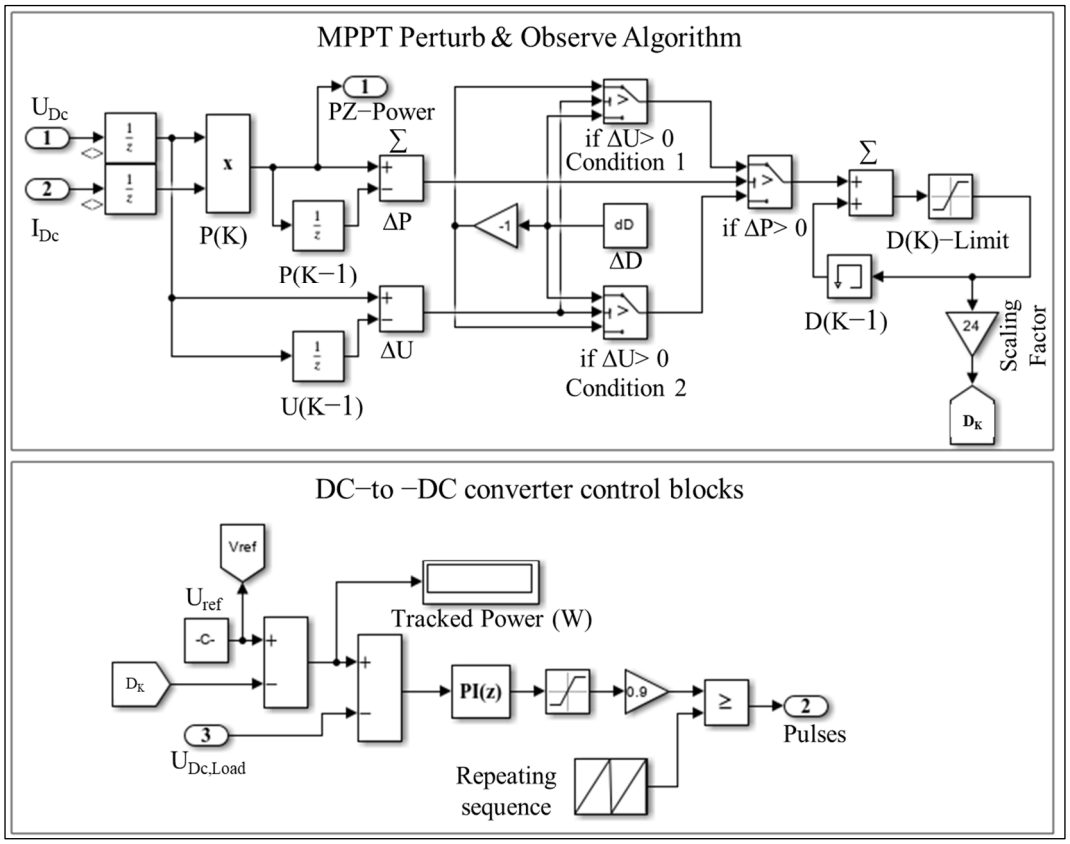

Figure 5. Implementation of the perturb and observe (P&O) MPPT algorithm with a closed-loop controller for a DC-to-DC converter.

The unit delay function block implements the previous sample $(k-1)$. The P&O algorithm uses the condition switch block to manage its three if–else conditions. Additionally, the block ΔD_B enables users to specify the perturbation step size of the duty cycle. An adder with a memory block manages the functions for the duty cycle's increase and decrease, ensuring consistency with the previous duty cycle, $D_B(k-1)$. A limit block, $D_B(k-1)$, is used to restrict the duty cycle within the range of 0.4–0.6, as reported in [43].

For D(k), multiplication by a constant gain of 24 represents the desired V_{ref} for the MPPT controller. This scaling factor is critical for ensuring that the system operates at the optimal voltage level to extract the maximum power from the vibration source, as well as aligns with the desired operating point.

In a closed-loop controller implementation using a buck-boost converter, the D_k generated from the P&O MPPT algorithm is multiplied by a constant gain to match the level of the control signal, U_D. The control signal is subtracted from the V_{ref} set reference voltage to satisfy the requirements of the load or storage system. The PI controller receives the loop error by subtracting the measured converter output voltage from the reference voltage, which adjusts the duty cycle for the PWM generator. On the basis of the feedback from the voltages, the controller continuously modifies the operating point of the DC-to-DC converter to maintain system operation at or near the reference voltage [40].

4. Simulation of Wind Vibrations Integrated with Piezoelectric Materials

In this section, the simulations explain how the proposed integration of PEHS with wind-induced mechanical vibrations effectively generated electrical energy. The goal was to improve the PEHS design. Table 1 lists the parameters used in the simulation analysis. The simulation focused on the first five cycles of the fundamental frequency for the vibrational wind force.

Table 1. Simulation parameters for the PEHS with vibrational wind force.

Definition	Value
Amplitudes of wind force (N)	200
Wind vibration speed (Hz)	50
Translational damper N(m/s)	100
Translational spring (N/m)	400
Mass for mechanical part (kg)	3.6
Rectifier switching frequency (Hz)	5000
Filter capacitor (μf)	4500
DC–DC converter switching frequency (Hz)	20,000
DC–DC converter inductance (μH)	45
DC–DC converter capacitor (μf)	100
R load (Ω)	4000

4.1. AC-to-DC Converter Based on Wind Energy Harvesting

A translational motion sensor was inserted to extract and convert signals between two mechanical translational nodes in accordance with velocity and position. The piezo stack is a piezoelectric sensor model. The piezo stack uses the translation damper and the translation spring to model its mechanical components. Figure 6 illustrates the electromechanical model of the wind energy harvester. In the piezoelectric model, the mass–spring damper system received a sinusoidal force input, whereas a sensor detected the electrical output of the piezoelectric element. This force caused displacement in the spring and damper, which in turn generated vibrations in the piezoelectric element. A sinusoidally varying AC voltage source was used to represent the electrical voltage that the piezoelectric effect generated.

The proposed framework simplified the process of exploring the effects of changing the mechanical vibrating source input parameters, such as displacement and frequency. The physical parameters, such as velocity, mass, force applied, and damping factor, can describe the wind-induced vibration. Several properties of the piezoelectric material underwent changes when subjected to a vibration source.

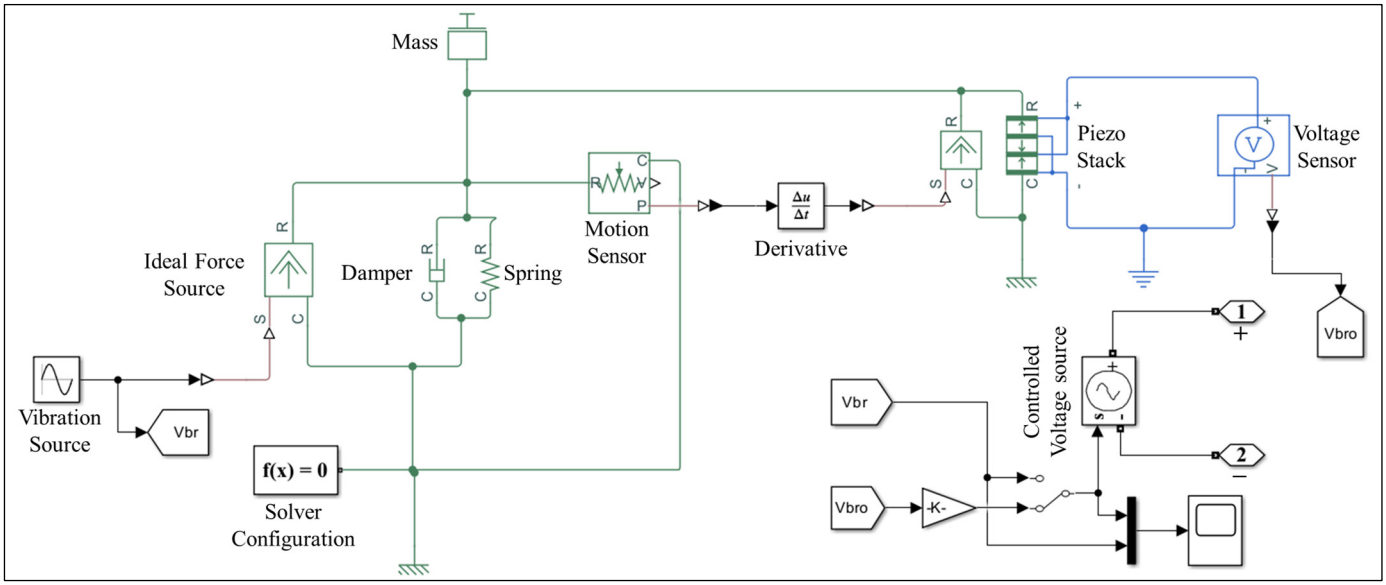

Figure 6. Piezoelectric wind-energy-harvesting simulation blocks.

These properties included the effective mass size, number of layers, charge constant, dielectric constant, elastic compliance, damping, and mechanical quality factor [34]. The piezoelectric material produced an electrical charge when exposed to mechanical stress [44]. The amount of electrical response depends on the displacement of pulsing of mechanical stress applied. When stress was applied to a piezoelectric material, the positive and negative charge centers within the crystal structure moved. This movement created an electric polarization and an electric potential across the material [8]. Thus, Figure 7 shows a comprehensive explanation of the mechanical and electrical AC-to-DC converters in Simulink.

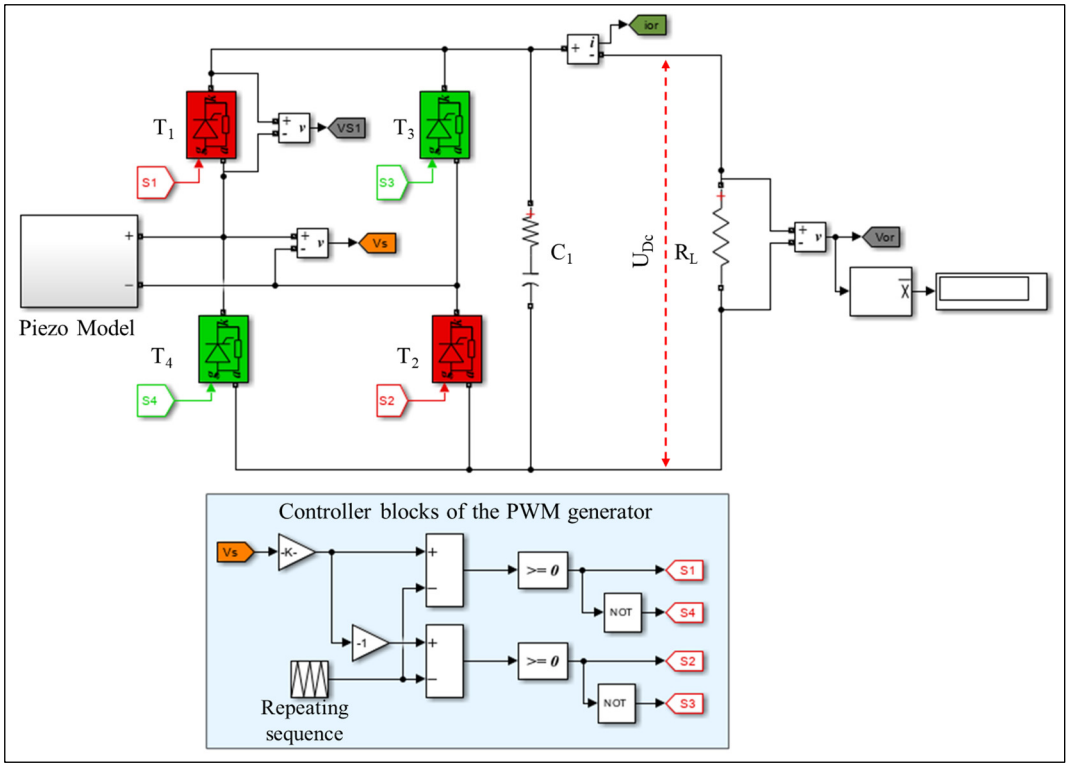

Figure 7. Simulation blocks of the AC–DC converter.

The rectifier switches used a PWM full-wave rectifier to reduce total harmonic distortions in the output waveform [40]. The rectifier passed the DC output voltage through a capacitive filter to minimize pulsation and reduce distortion in the DC voltage.

Table 2 shows the simulation results for the maximum and minimum voltages of an AC–DC converter with two excitation frequency ranges. The maximum voltage and minimum voltage were recorded at 0.09 and 1 s, respectively.

Table 2. Minimum and maximum voltages of an AC–DC converter with various vibration frequencies.

Amplitude of Wind Force (m/s^2)	Excitation Frequency Range	Vibration Frequency (Hz)	Δt = 1.16 s	
			V_{DCMax}	V_{DCMin}
200	Low	0.5	71	7.6
		1	71	7.6
		1.5	71	7.6
		2	71	7.6
	High	15	75	45
		25	80	58
		40	80	66
		50	80	70
		150	82	80

The data listed in Table 2 show the impact performance across a spectrum of low and high vibration frequencies. A low excitation frequency and high vibration frequency were used to demonstrate the variability in the studied simulation model in terms of better aligning various excitation frequency sources.

In the context of PEHS technology, using a sinusoidal waveform with a frequency greater than 5 Hz was more relevant to the ideal [35]. In such cases, PEHS often operates at higher frequencies to maximize the energy conversion efficiency. In addition, the system might be exposed to higher-frequency components, such as those resulting from rotational resonances or other environmental factors.

Vehicle-generated wind can produce excitation frequencies exceeding 15 Hz due to differences in vehicle size and speed, unlike natural wind, which typically has a dominant vibration frequency below 5 Hz [45]. This provides a comprehension performance analysis for the PEHS model. It confirms its suitability for simulating more realistic vibration scenarios, such as vibration sources of wind from passing cars on the highway, which can generate excitation frequencies. The dominant frequency can vary depending on factors such as wind speed, terrain, and the structure's height [35].

Therefore, in order to better align with the typical wind excitation scenarios, additional simulations at frequencies below 5 Hz were conducted, which revealed how the system performed under more realistic conditions, where the vibration wind excitation frequency was much lower. At low ranges of excitation frequencies of 0.5 and 1 Hz, Figures 8 and 9 show the output voltage, current, and switch pulse of the AC–DC converter based on the input sinusoidal frequencies.

Figures 10–12 show the output voltage, current, and switch pulse of the AC–DC converter, respectively, on the basis of input sinusoidal frequencies of 15, 50, and 150 Hz. The closed-loop buck-boost converter then received this DC voltage and adjusted the DC voltage level to meet the load requirements.

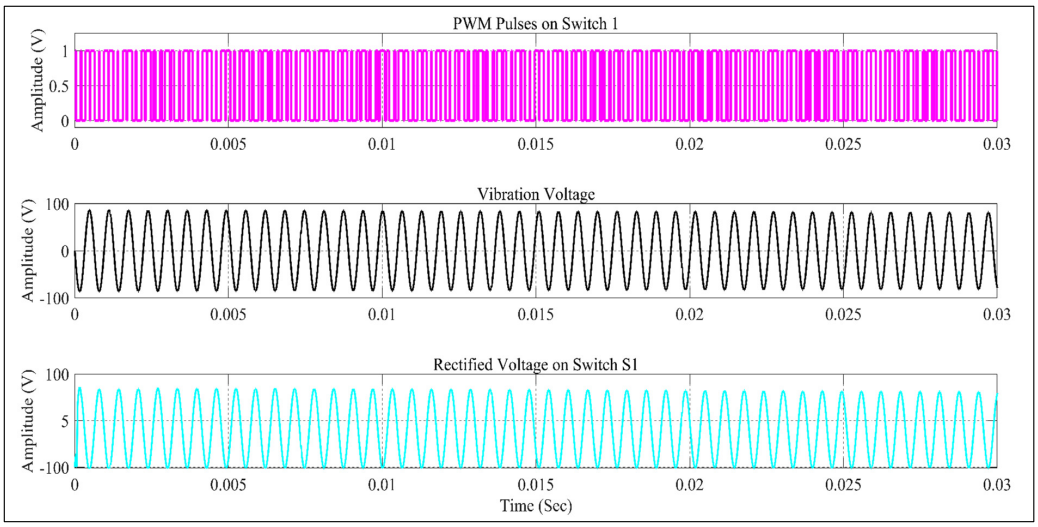

(**a**) PWM signal and voltage characteristics at Switch 1.

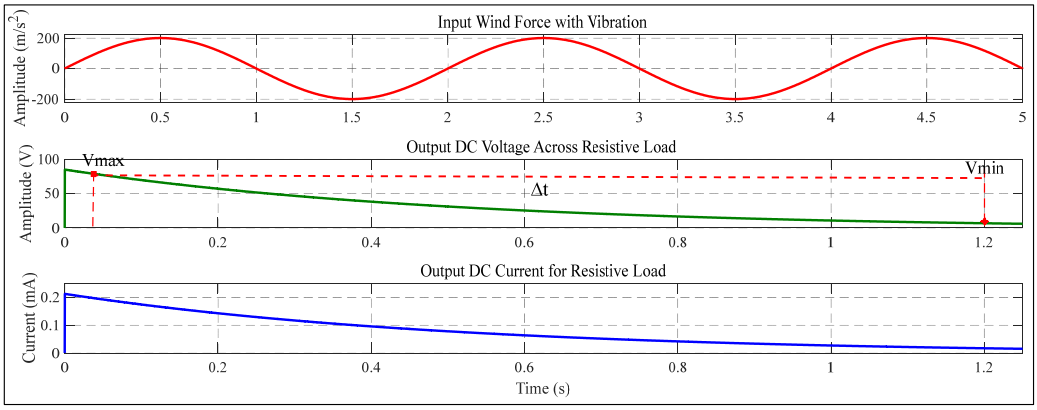

(**b**) The impact of vibration-induced wind force and cell output voltage current across resistive loads.

Figure 8. Rectifier voltage, current, and vibration force at a vibration frequency of 0.5 Hz.

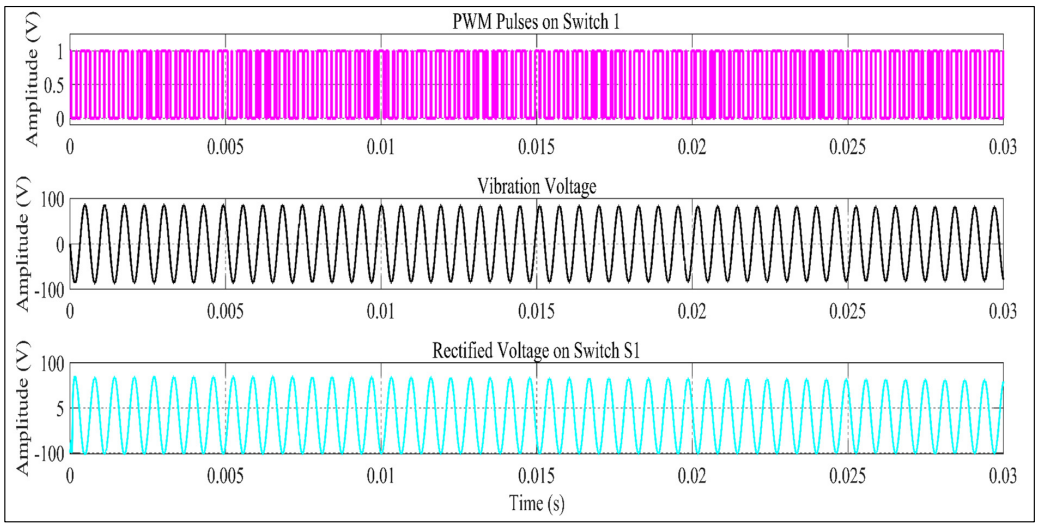

(**a**) PWM signal and voltage characteristics at Switch 1.

Figure 9. *Cont.*

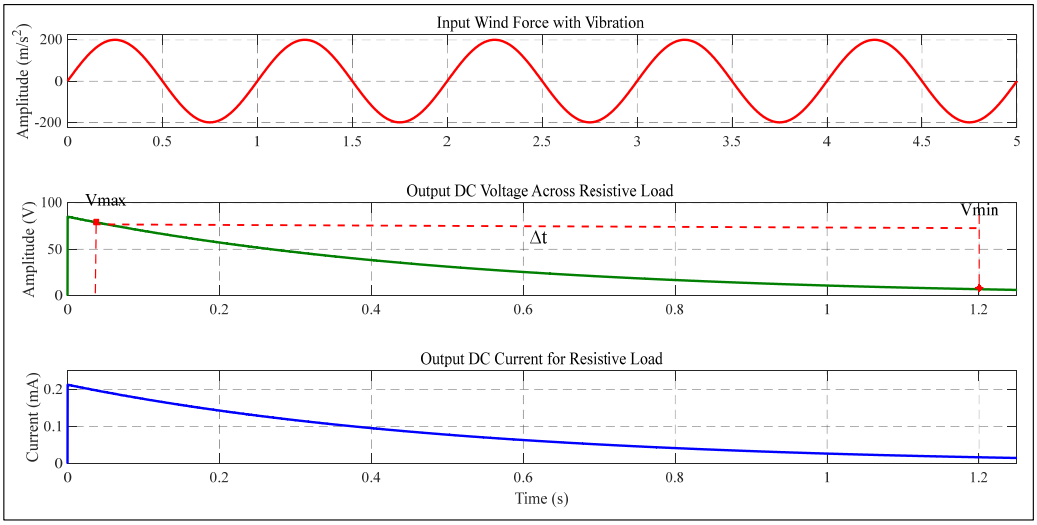

(**b**) The impact of vibration-induced wind force and cell output voltage current across resistive loads.

Figure 9. Rectifier voltage, current, and vibration force at a vibration frequency of 1 Hz.

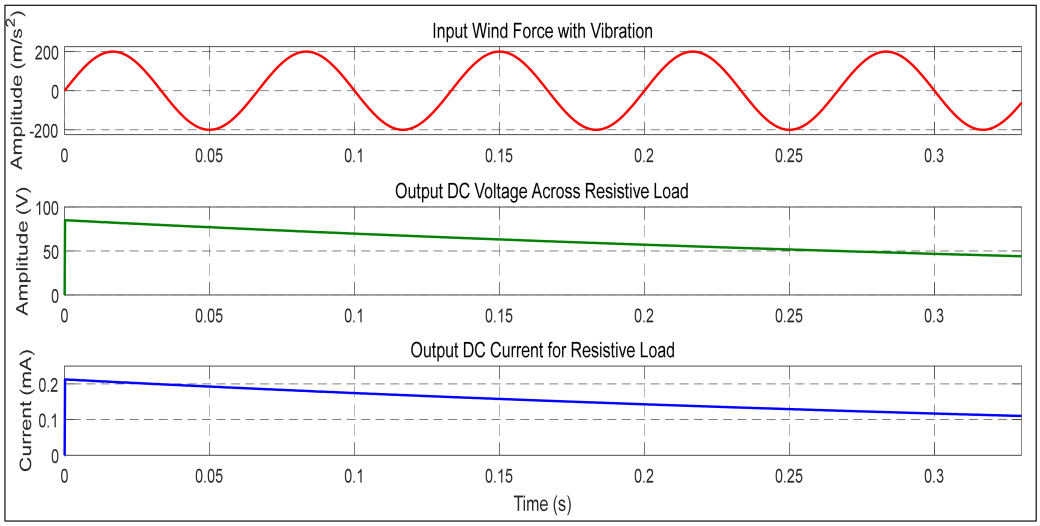

(**a**) PWM signal and voltage characteristics at Switch 1.

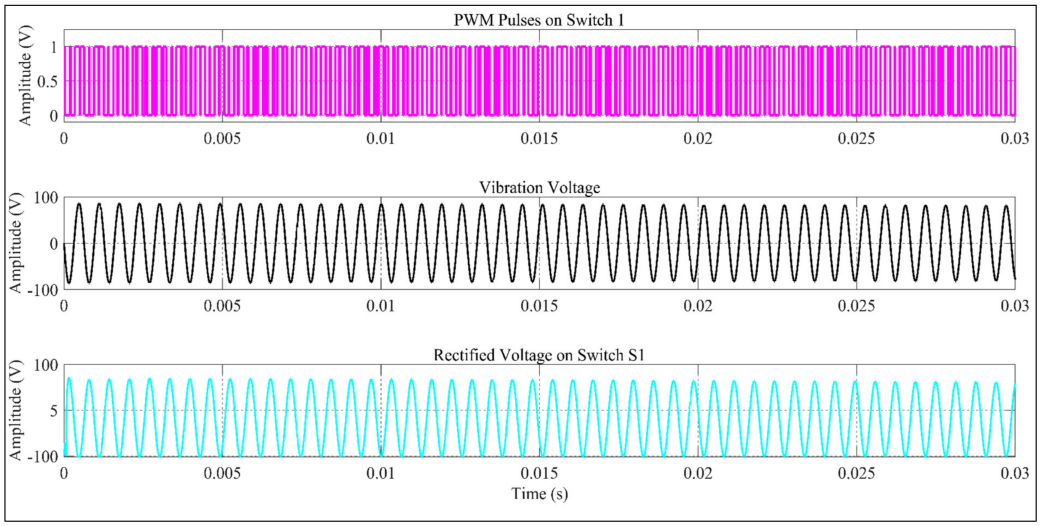

(**b**) The impact of vibration-induced wind force and cell output voltage current across resistive loads.

Figure 10. Rectifier voltage, current, and vibration force at a vibration frequency of 15 Hz.

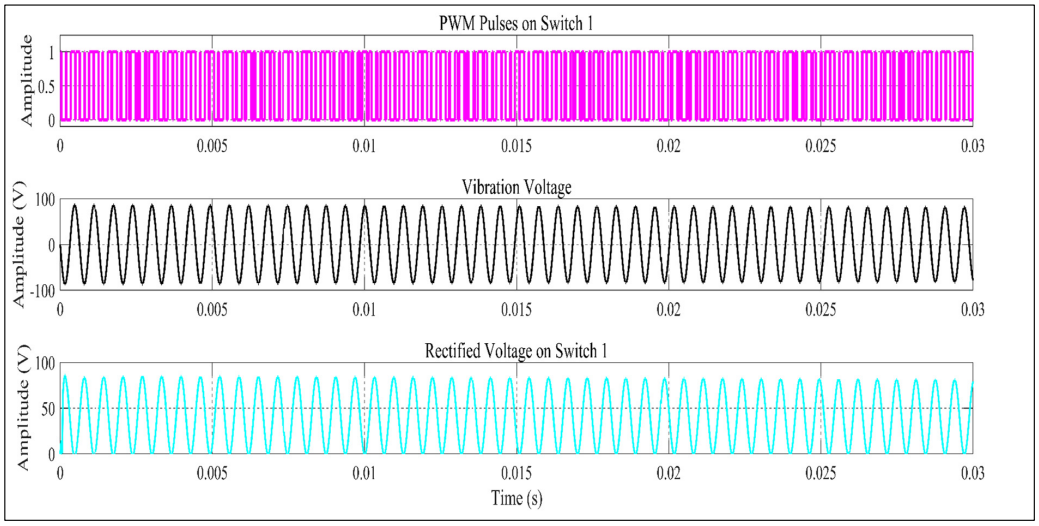

(**a**) PWM signal and voltage characteristics at Switch 1.

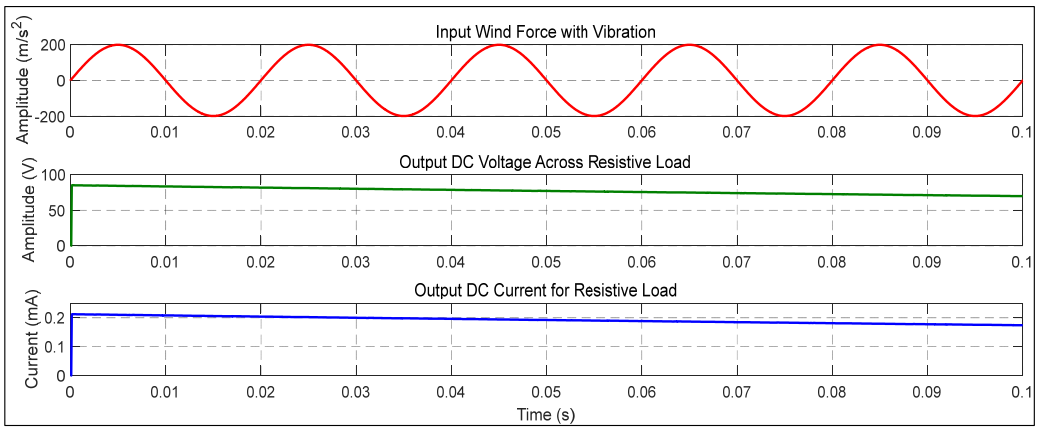

(**b**) The impact of vibration-induced wind force and cell output voltage current across resistive loads.

Figure 11. Rectifier voltage, current, and vibration force at a vibration frequency of 50 Hz.

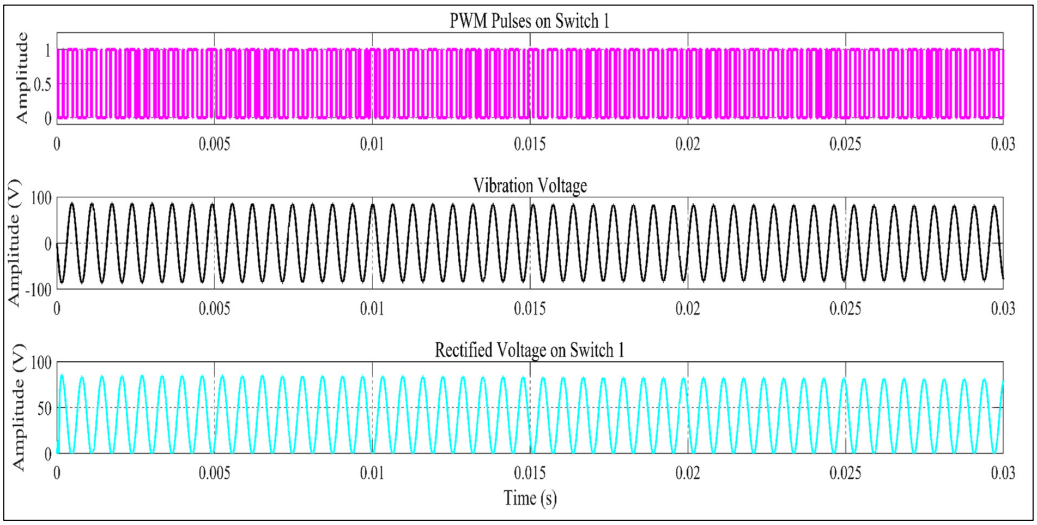

(**a**) PWM signal and voltage characteristics at Switch 1.

Figure 12. *Cont*.

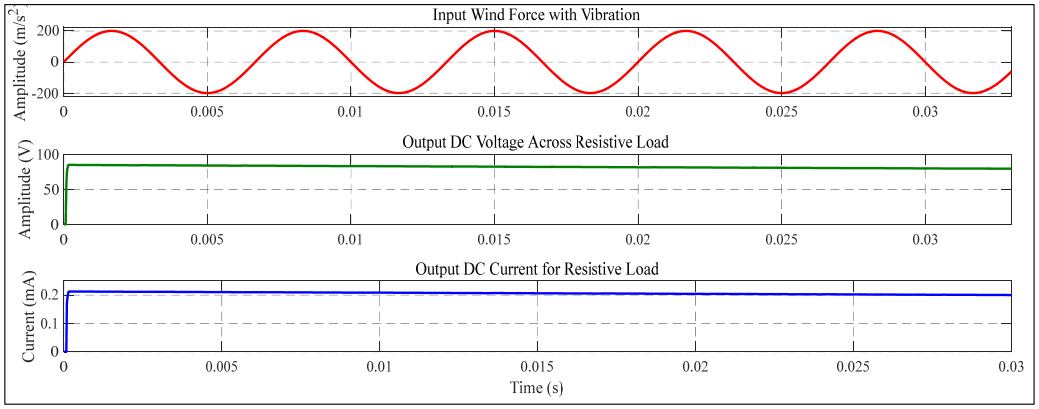

(**b**) The impact of vibration-induced wind force and cell output voltage current across resistive loads.

Figure 12. Rectifier voltage, current, and vibration force at a vibration frequency of 150 Hz.

Figure 13 shows the simulation blocks of the closed-loop buck-boost converter. The evolution of closed-loop controllers for DC-to-DC converters played a significant role in the overall performance of the proposed energy conservation system.

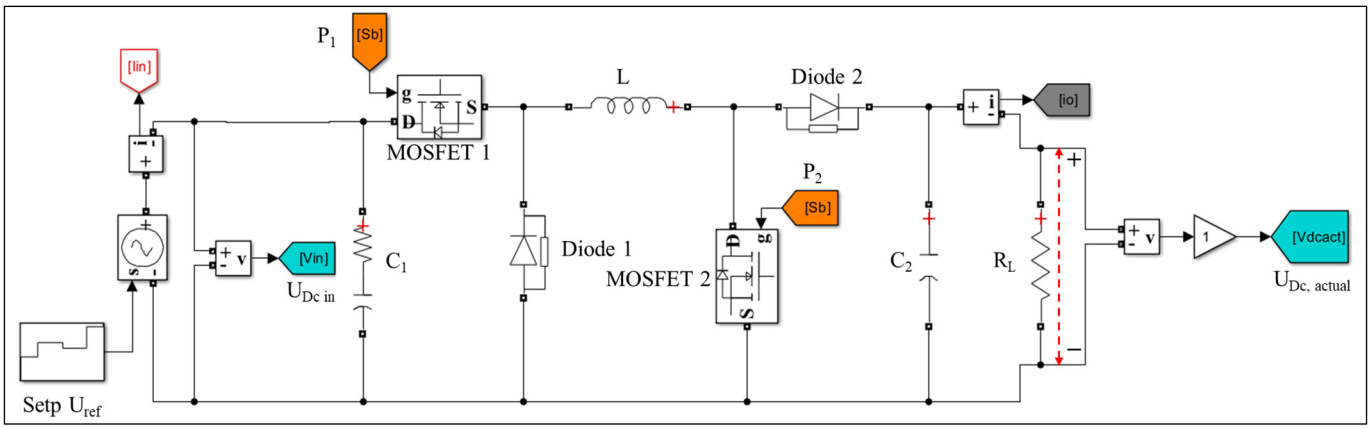

Figure 13. Closed-loop buck-boost converter.

Figure 14 illustrates the performance of the DC-to-DC converter controller, which continuously modified the output voltage according to the reference voltage, set at 24 V.

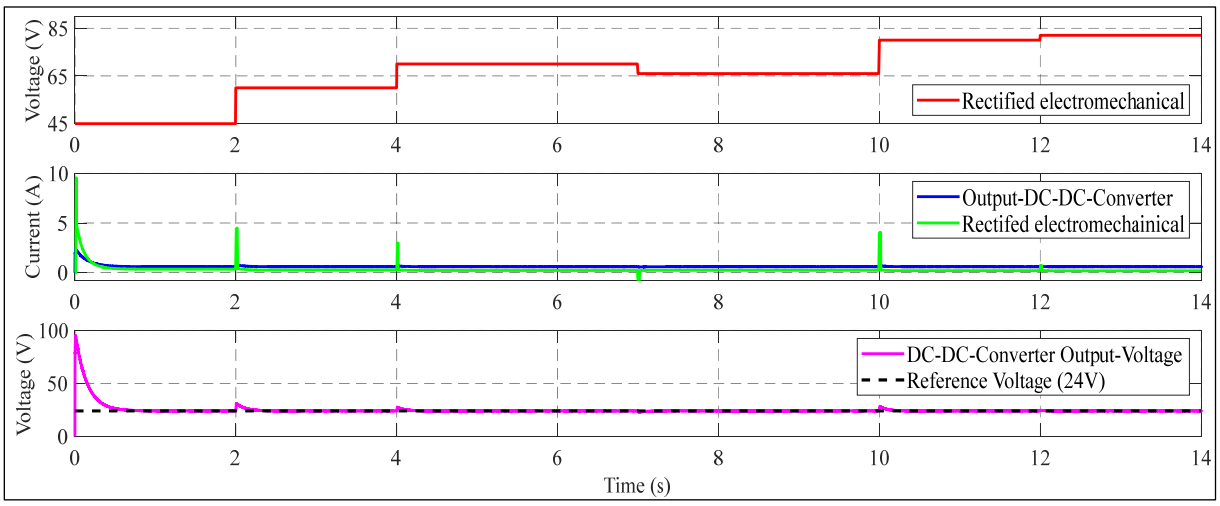

Figure 14. The performance of the DC-to-DC converter controller with a reference voltage set at 24 V.

4.2. Simulation of the Proposed Integrated Piezoelectric Energy-Harvesting Cell

To simulate an integrated PEHS, we combine an AC–DC converter, a buck-boost converter based on the P&O MPPT algorithm, and a piezoelectric energy-harvesting source. The closed-loop DC–DC converter changed its duty cycle on the basis of the input voltage and current from a full-wave rectifier, whereas the controller continuously tracked the set reference voltage. This made it flexible for changing environmental conditions, but there could be oscillations around the maximum power point.

Figure 15 illustrates the wind vibration energy-harvester system, which fed the current and voltage outputs from the PWM rectifier to the P&O MPPT buck-boost converter, specifically focusing on the conversion of the mechanical impact of wind into electrical energy.

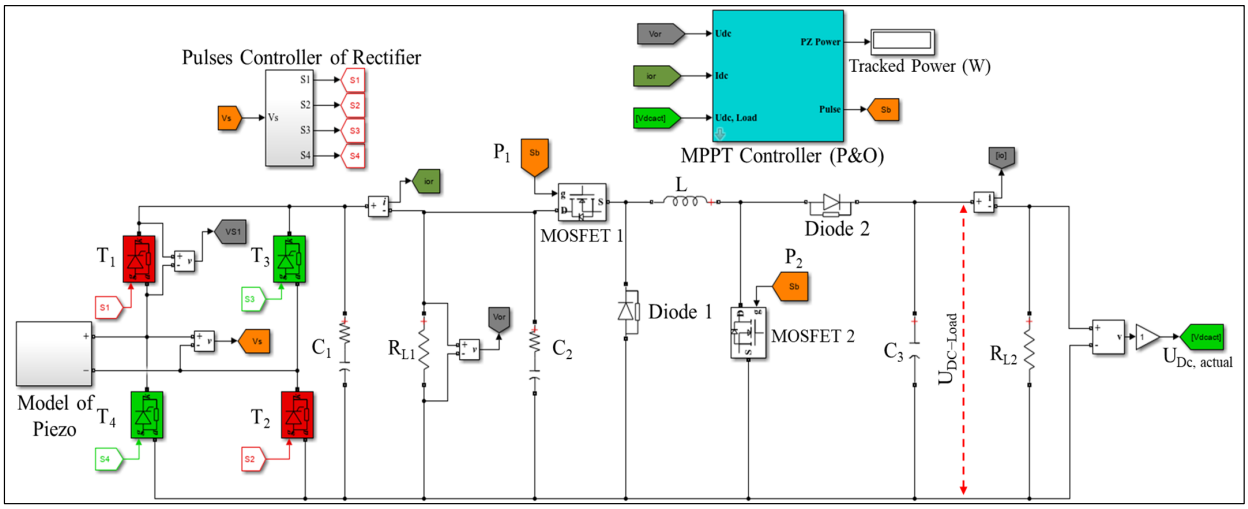

Figure 15. Wind vibration energy harvester with closed-loop controllers in buck-boost converters (P&O MPPT).

The closed-loop P&O MPPT DC–DC converter is one of the most frequently used converters [27]. The DC–DC converter continuously regulated the operating point to ensure that it operated at its maximum level, which depended on the rectified voltage and current of the PEHS sources. In addition, the closed loop was responsible for setting the required output voltage. Figure 16 shows the DC output voltage of the PEHS over time under a constant wind impact force and a 50 Hz vibration frequency. This can provide good insight into the performance of wind-energy-harvester systems that track the set reference voltage.

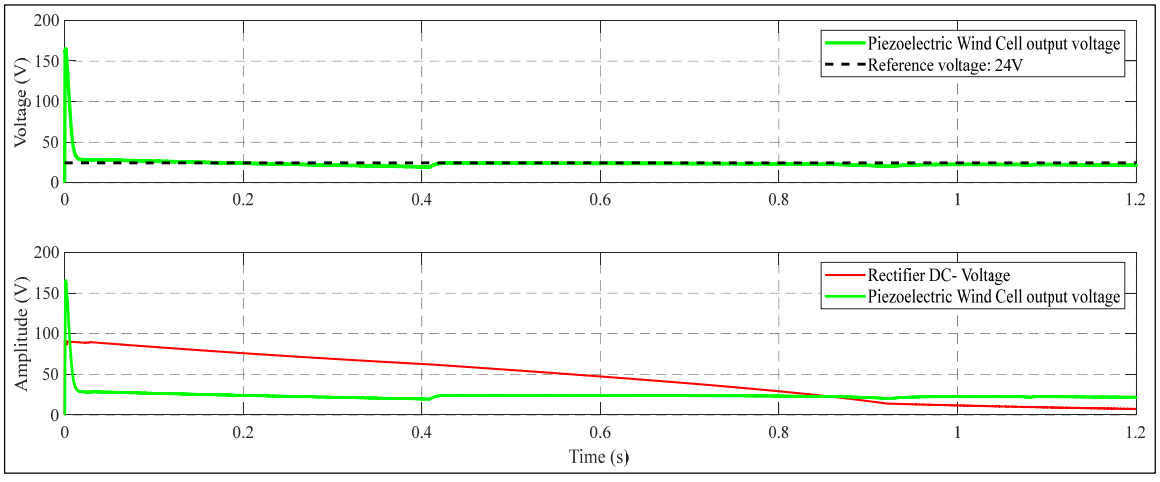

Figure 16. DC output voltage of PEHS with a closed-loop P&O MPPT buck-boost converter.

5. Discussion

The proposed design of the PEHS approach, which incorporates a closed-loop buck-boost converter based on the P&O MPPT algorithm, represents a substantial improvement in the area of vibrational energy-harvesting technology. The proposed design of the PEHS operates at a wide range of vibration frequencies, which, together with its effective power conversion and consistent output, make it a very favorable option for sustainable energy production.

Figures 10–12 show the rectifier voltage, current, and vibration force for input frequencies of 15 Hz, 50 Hz, and 150 Hz, respectively. The results indicated the ability of the proposed PEHS to efficiently transform generated voltages under different vibration frequencies. As shown in Figures 8 and 9, the AC-to-DC converter section stability increased the rectified voltage, which meant that it could start transferring power even at lower vibration frequencies. These results align with previous studies on energy-harvesting devices, which validates the rectifier's appropriateness for situations that include low-frequency vibrations. However, more research needs to prioritize investigating the rectifier's performance at low vibration frequencies, varying wind force amplitudes, and long-term vibration. Additionally, it should explore the integration of the rectifier with energy storage devices to enhance its suitability in dynamic and real-world settings.

The output demonstrated greater and more consistent voltages at a frequency of 50 Hz, suggesting that this frequency range is best for achieving peak performance. The system exhibited stable operation at a frequency of 50 Hz, which is typically used in several practical applications.

As shown in Figure 11, the AC-to-DC converter section effectively managed higher frequencies, resulting in a notable amplification in the output voltage. However, the heightened wind vibration force may induce supplementary mechanical strains, although the AC-to-DC converter seemed to handle it effectively. As shown in Figure 14, the proposed buck-boost converter control approach exhibited notable performance in terms of the output voltage matching the reference voltage set. Despite fluctuations in the input voltage level, the controller continuously maintained an output voltage that reflected the robust and reliable performance of the suggested control method. Furthermore, the ability of the closed-loop controller to promptly adjust the output voltage signified an effective feedback system, which is crucial for sustaining stability in dynamic circumstances. The closed-loop system ensured a consistent and steady DC output, which is crucial for ensuring a dependable power supply to the load. Despite fluctuations in the input voltage level, the controller continuously maintained an output voltage that reflected the strong and dependable performance of the proposed control method.

Furthermore, as shown in Figure 16, the ability to control and quickly modify the output voltage signified an effective feedback system, which is crucial for sustaining stability in dynamic circumstances. The closed-loop system guaranteed a steady DC output, which is essential for achieving optimal power delivery to the load.

Moreover, Figure 17 and Table 3 present the recommended electric circuit diagram and real-time circuit components for the proposed PEHS design, respectively. Figure 17 shows the diagram of the suggested circuit design, which provides a visual representation of the organization and interconnections of the necessary components for the system. Table 4 provides a comprehensive list of the individual components used in the design, including piezoelectric transducers, PWM-controlled rectifiers, DC–DC converters, and lithium batteries. The circuit diagram in Figure 17 and the detailed component breakdown in Table 3 provide a comprehensive reference for constructing the proposed PEHS.

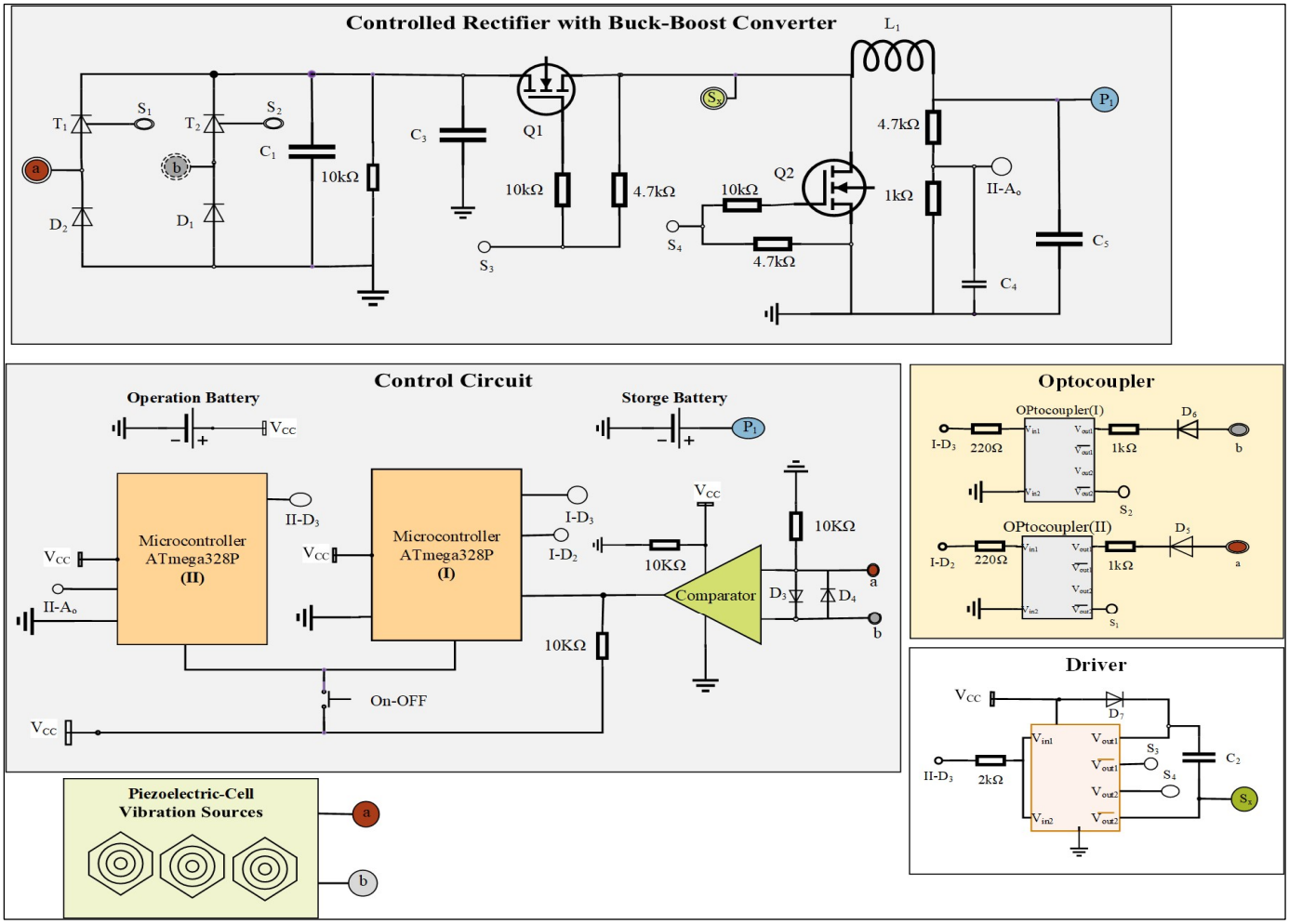

Figure 17. Comprehensive diagram of the recommended design for the proposed PEHS.

Table 3. The recommended electric components in the proposed design of the PEHS.

Section	Components	Location	Manufacturer and Specifications	Number	Approximal Cost (in USD)
Source of energy	Piezo transducer	-	-	12	36 (3 each)
Rectifier	Microcontroller	I	ATmega328P	1	2.5
	Optocoupler	I, II	PC817	2	1.4 (0.7 each)
	Thyristor (SCR)	T_1, T_2	TYN1225	2	5 (2.5 each)
	Comparator	-	LM339	1	0.6
	Diode	D_1, D_2, D_3, D_4, D_5, D_6	IN4007	6	1.5 (0.25 each)
	Resistor	-	Ω to Ωk	9	1.8 (0.2 each)
	DC capacitors	C_1	470 µf	1	0.5 (0.5 each)
DC–DC Auto Voltage Converter + MPPT	Microcontroller	II	ATmega328P	1	2.5
	Capacitors	-	C_3, C_5 = 3300 µf C_4 = 10 pf C_2 = 100 µf	2	1
	Resistor	-	-	7	1.4 (0.2 each)
	MOSFET	Q_1, Q_2	IRFZ44Zl	2	1.5 (0.75 each)
	MOSFET-driver	driver	IR2103	1	0.5
	diode	D_7	IN4007	1	0.25
	Inductor	L1	220 mH	1	1.25
Energy storage	Lithium battery	Storge battery	3.3 V, 350 mA	1	7.5
Operation battery	Lithium battery	Operation battery	5 V, 200 mA	1	7.5

Table 4. Comparison of the main parts of PEHS established on a closed-loop P&O MPPT DC–DC converter against energy harvesters' existing state-of-the-art systems.

Reference No.	Rectifier Structure	DC–DC Converter	SimulationDesign	Experimental Design
Ajitsaria et al., 2007, [28]	Uncontrolled bridge diodes	Not used	Yes	No
Boisseau et al., 2011, [34]	None	None	Yes	No
Balato et al., 2018, [27]	Uncontrolled bridge diodes	P&O MPPT closed-loop boost converter	Yes	Yes
Proposed system	PWM rectifier bridge IGBT	P&O MPPT closed-loop buck-boost converter	Yes	No

The estimated costs for components can vary depending on the provider and geographical location. At our location in Iraq, the total estimated cost of all components would be approximately USD 73.

5.1. Limitations of the Proposed PEHS

The most striking limitation is the source of vibration, which has a significant effect on the proposed PEHS. The effectiveness of the PEHS is intrinsically contingent upon the presence and regularity of ambient wind-induced vibrations or vibration sources. In environments where these vibrations occur sporadically or are feeble, the system can have difficulty producing an adequate amount of electricity, thereby restricting its reliability in such environments.

Piezoelectric materials are susceptible to environmental conditions, such as temperature and humidity, which can have an impact on the energy conversion efficiency and durability as time passes. The PEHS primarily targets low-power applications, leading to restricted power output. This constraint may limit its use in situations that require higher energy outputs, restricting it to certain categories of low-power electronic equipment. Moreover, another limitation is energy storage, as well as the cycle of charging and discharging batteries.

5.2. A Comparison with Previous State-of-the-Art and Broader Contexts

The findings indicated that the proposed design of the PEHS, which incorporates a closed-loop perturbation and an observed MPPT buck-boost converter, was remarkably efficient in converting the mechanical vibration force at various frequencies into a consistent supply of electrical energy. This feature is crucial for applications in domains with fluctuating and uncertain sources of vibrational energy, such as equipment, structures, and transportation systems.

Previous studies have often concentrated on either low-frequency or high-frequency vibration energy-harvesting devices, which yield different levels of achievement. The present paper demonstrated a significant enhancement in its ability to handle a broad variety of vibration frequencies while maintaining a consistent output voltage.

This increase effectively bridged the gap between various operating situations. In addition, the use of advanced MPPT techniques improved the overall efficiency, which is a significant improvement over simpler and less effective systems. The broad and significant implications of this study can be summarized as follows:

- Improved energy solutions. The improved energy solution system efficiently converted vibrational energy into electrical energy. This design can offer dependable power sources for remote sensors, IoT devices, and other low-power applications, reducing reliance on batteries or traditional power sources.
- Sustainable energy sources. The use of ambient vibrations for energy harvesting is compatible with sustainable energy objectives, offering an environmentally friendly substitute for traditional energy sources while diminishing eco-friendly alternatives.
- Scalability and flexibility. The suggested design of the PEHS has the potential to be expanded to handle larger applications, enabling the provision of power solu-

tions for more extensive infrastructure. This technology's ability to accommodate a broad variety of frequencies makes it extremely flexible for many industrial and commercial applications.

Table 4 compares the PEHS with a closed-loop P&O MPPT DC converter with available state-of-the-art systems. The comparison table contains the following information: types of rectifiers, DC-to-DC converters, and design applicability.

The proposed energy-harvesting system stands out because of its use of a PWM-IGBT bridge rectifier with a P&O MPPT closed-loop buck-boost converter. This structure can provide efficiency in power conversion management compared with systems employing uncontrolled bridge diodes with DC–DC converters.

In contrast to the system explained in [27], the proposed PEHS did not undergo full experimental testing, despite partial experimental testing via simulation and validation, which provided a thorough evaluation of its performance mathematically. This limitation underscores the importance of further experimental validation to assess its viability in real time as a prototype design. However, the proposed system shows promise because of its advanced components and comprehensive assessment through simulation compared with existing state-of-the-art systems.

Results in Table 5 show the improved efficacy of the proposed dynamic simulation model of the PEHS compared to existing PEHS models in the literature. The suggested PEHS operates within a larger, lower frequency range of 15–50 Hz, producing an elevated AC output voltage of 75 V and a substantially increased power output of 500 mW. These measurements far surpass those of the other systems examined, including those of Ericka et al. [9] and Barton et al. [11], which operate at elevated frequencies and produce diminished voltages and power.

Table 5. Comparison of the main characteristics of the proposed PEHS with existing systems in the literature.

Reference No.	Vibration Frequency (Hz)	AC Output Voltage of Piezoelectric Transducer	Maximum Power Output (mW)	R Load (kΩ)
Ericka et al., 2005, [9]	2580	18.36	56	1.8
Barton et al., 2009, [11]	80	1.2	2	333
Wang et al., 2022, [10]	150	17	27	11
Proposed system simulation	15~50	75	500	4

Figure 18 illustrates the effectiveness of the suggested PEHS diagram in comparison to other PEHS models, emphasizing the maximum actual power and open-circuit voltage. In Figure 18a, the proposed circuit diagram demonstrates a significant increase in power production, surpassing current methods, especially at lower vibration frequencies, making it more appropriate for real-world energy-harvesting applications.

The proposed circuit diagram assumes a charging current of 175 mA, which is safer and less stressful for the lithium battery. In addition, the PEHS diagram produces 500 mW of real power delivery to a lithium battery.

Figure 18b shows a significant increase in the open-circuit voltage of the suggested PEHS, indicating improved efficiency in the conversion of mechanical energy to electrical energy. These enhancements are based on improvements in the suggested circuit design, making the system more efficient for powering external loads and energy storage, ensuring a dependable and sustainable power source.

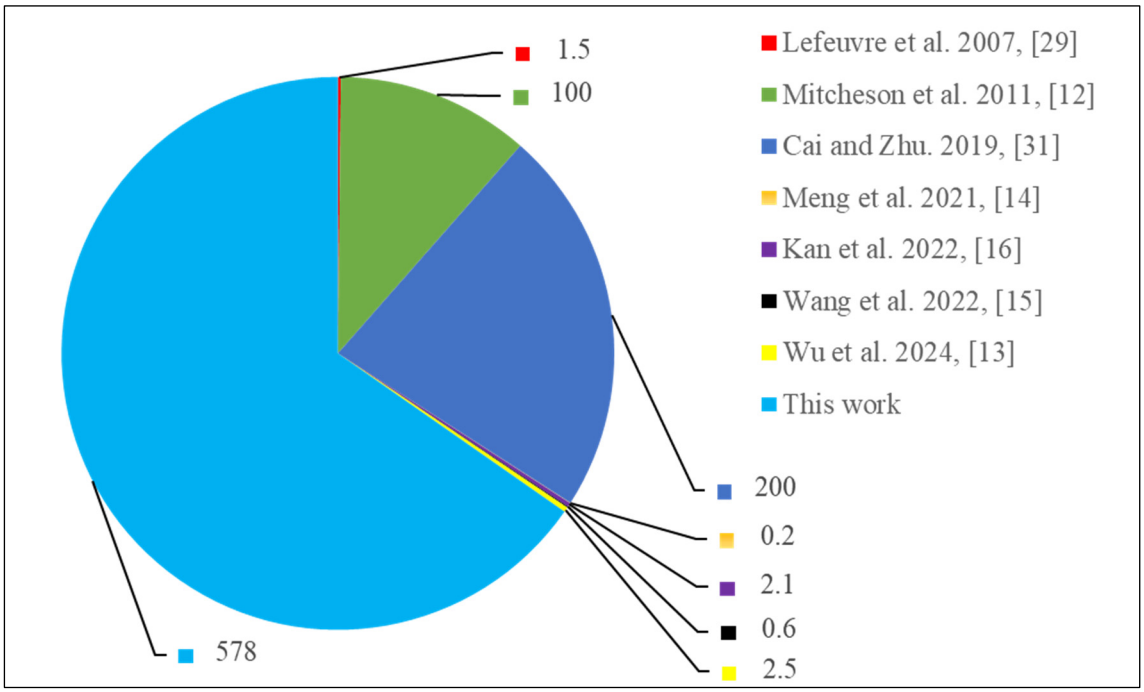

(**a**) Maximum real power produced (mW).

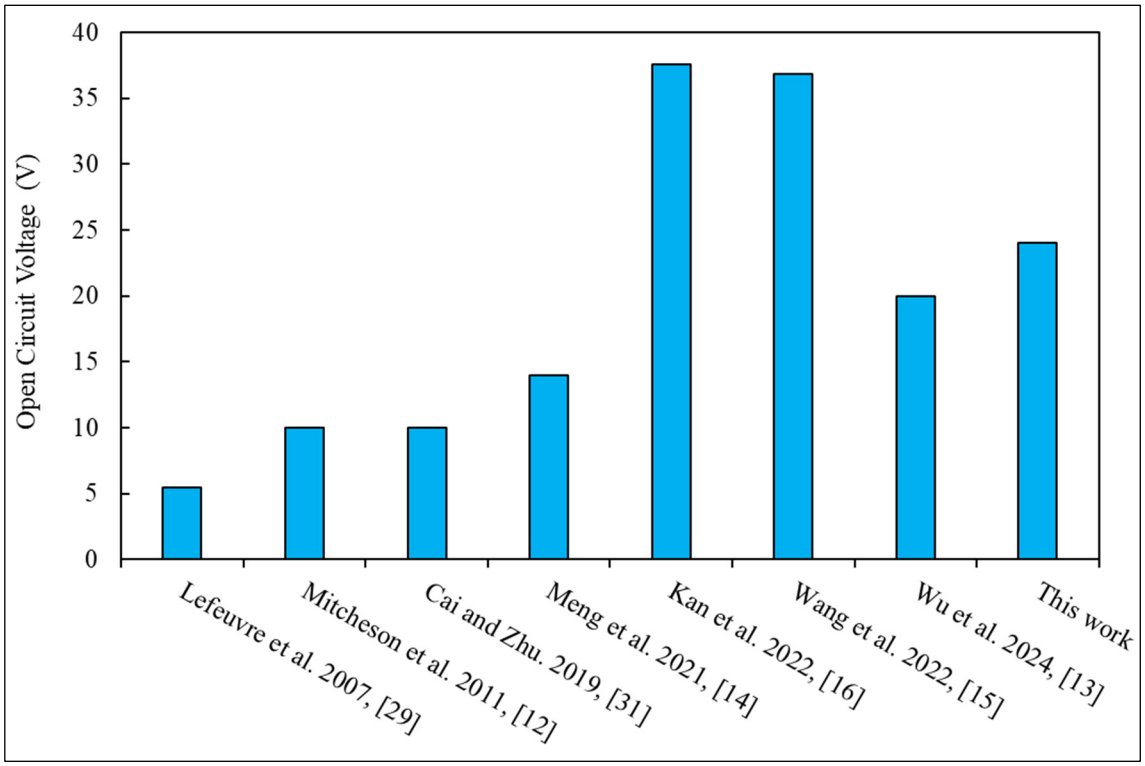

(**b**) Open-circuit voltage of piezoelectric transducer.

Figure 18. Performance comparison of the suggested PEHS circuit diagram with systems available in the literature from the point of view of real power and open-circuit voltage.

6. Conclusions

This article introduced a dynamic simulation model for a piezoelectric vibration energy-harvesting system based on wind vibration energy as a source of mechanical energy. The proposed model has integrated electrical circuits, such as an AC-DC converter, a

closed-loop buck-boost converter, and an MPPT algorithm. A detailed description of the dynamic simulation performance was provided, in addition to a brief overview of each part of the system. Specifically, the MPPT-equipped piezoelectric harvester generated a significantly higher DC electrical output voltage when it encountered a resistive load of 4 kΩ. This makes it a good choice for a wide range of low-voltage applications.

Notably, the closed-loop AC-to-DC converter based on the perturb and observe MPPT harvester demonstrated more stable output voltages, and the closed-loop DC-to-DC converter provided better tracking of the reference set values. This demonstrates that the vibration energy harvester with a closed-loop AC-to-DC converter, as well as the perturbation and observation MPPT, produced better performance than the systems available in the literature.

To improve the results of this study, some recommendations for future extensions of this work are provided. The same simulation should be extended with a practical wind spectrum excitation dataset, which provides deeper insights into real-world performance. Using wind data and conducting field experiments to verify the accuracy of the simulation results and enhance the system's design under real wind conditions would be beneficial. Additional studies might investigate the optimization of electrical components using actual wind excitation situations, resulting in enhanced efficiency and dependability.

Author Contributions: A.K.A.: conceptualization, writing (original draft), methodology, investigation, writing (review and editing), software, and validation. A.A.A.: review and editing. A.H.M.: review and validation. All authors have read and agreed to the published version of the manuscript.

Funding: This research received no external funding.

Data Availability Statement: As the corresponding authors of this paper, we declare that we will upload all the simulation files and supporting data after the paper's publication.

Acknowledgments: The authors express their profound appreciation to the Middle Technical University, Institute of Technology, Baghdad, Iraq, for their significant aid and support over the course of this work. Their administrative and technical assistance has been critical to the successful completion of this study.

Conflicts of Interest: The authors declare that they have no conflicts of interest.

References

1. Adom, P.K. The Transition between Energy Efficient and Energy Inefficient States in Cameroon. *Energy Econ.* **2016**, *54*, 248–262. [CrossRef]
2. Adom, P.K.; Adams, S. Energy Savings in Nigeria. Is There a Way of Escape from Energy Inefficiency? *Renew. Sustain. Energy Rev.* **2018**, *81*, 2421–2430. [CrossRef]
3. Amjadi, G.; Lundgren, T. Is Industrial Energy Inefficiency Transient or Persistent? Evidence from Swedish Manufacturing. *Appl. Energy* **2022**, *309*, 118324. [CrossRef]
4. Butt, O.M.; Ahmad, M.S.; Che, H.S.; Rahim, N.A. Usage of On-Demand Oxyhydrogen Gas as Clean/Renewable Fuel for Combustion Applications: A Review. *Int. J. Green Energy* **2021**, *18*, 1405–1429. [CrossRef]
5. Koszalka, G.; Hunicz, J. Comparative Study of Energy Losses Related to the Ring Pack Operation in Homogeneous Charge Compression Ignition and Spark Ignition Combustion. *Energy* **2021**, *235*, 121388. [CrossRef]
6. Pao, L.Y.; Johnson, K.E. Control of Wind Turbines Recent Developments. *Control Syst. Mag.* **2011**, *31*, 44–62. [CrossRef]
7. Akkaya Oy, S.; Özdemir, A.E. Piezoelectric-Based Low-Power Wind Generator Design and Testing. *Arab. J. Sci. Eng.* **2018**, *43*, 2759–2767. [CrossRef]
8. Dell'Anna, F.G.; Dong, T.; Li, P.; Wen, Y.; Yang, Z.; Casu, M.R.; Azadmehr, M.; Berg, Y. State-of-the-Art Power Management Circuits for Piezoelectric Energy Harvesters. *IEEE Circuits Syst. Mag.* **2018**, *18*, 27–48. [CrossRef]
9. Ericka, M.; Vasic, D.; Costa, F.; Poulain, G. Predictive Energy Harvesting from Mechanical Vibration Using a Circular Piezoelectric Membrane. In Proceedings of the IEEE Ultrasonics Symposium, Rotterdam, The Netherlands, 18–21 September 2005; Volume 2, pp. 946–949.
10. Wang, W.; Yang, T.; Chen, X.; Yao, X. Vibration Energy Harvesting Using a Piezoelectric Circular Diaphragm Array. *IEEE Trans. Ultrason. Ferroelectr. Freq. Control* **2012**, *59*, 2022–2026. [CrossRef]
11. Energy, R.; Barton, D.A.W.; Burrow, S.G.; Clare, L.R. Energy harvesting from vibrations with a nonlinear oscillator. In Proceedings of the ASME 2009 International Design Engineering Technical Conferences & Computers and Information in Engineering Conference, San Diego, CA, USA, 30 August–2 September 2009.

12. Dicken, J.; Mitcheson, P.D.; Stoianov, I.; Yeatman, E.M. Power-Extraction Circuits for Piezoelectric Energy Harvesters in Miniature and Low-Power Applications. *IEEE Trans. Power Electron.* **2012**, *27*, 4514–4529. [CrossRef]
13. Wu, W.; Pan, Z.; Zhou, J.; Wang, Y.; Ma, J.; Li, J.; Hu, Y.; Wen, J.; Wang, X. Wind-Speed-Adaptive Resonant Piezoelectric Energy Harvester for Offshore Wind Energy Collection. *Sensors* **2024**, *24*, 1371. [CrossRef] [PubMed]
14. Meng, X.K.; Lu, Z.; Dai, H.L.; Abdelkefi, A. Comparative Experimental Investigation and Effectiveness of Sphere- and Cylinder-Based Piezoelectric Energy Harvesters. *Smart Mater. Struct.* **2021**, *30*, 08LT01. [CrossRef]
15. Yu, G.; He, L.; Wang, S.; Tian, X.; Zheng, X.; Cheng, G. Experiments and Analysis of a Nonlinear Sickle-Shaped Cantilever Beam Piezoelectric Energy Harvester for Wind Energy Harvesting. *Phys. Status Solidi Appl. Mater. Sci.* **2022**, *219*, 2200363. [CrossRef]
16. Kan, J.; Wang, J.; Wu, Y.; Chen, S.; Wang, S.; Jiang, Y.; Zhang, Z. Energy Harvesting from Wind by an Axially Retractable Bracket-Shaped Piezoelectric Vibrator Excited by Magnetic Force. *Energy* **2022**, *240*, 122495. [CrossRef]
17. Zhao, Z.; Dai, Y.; Dou, S.X.; Liang, J. Flexible Nanogenerators for Wearable Electronic Applications Based on Piezoelectric Materials. *Mater. Today Energy* **2021**, *20*, 100690. [CrossRef]
18. Wang, P.; Xiao, Y.; Wu, N. Electrical Power Generation Using Dynamic Piezoelectric Shear Deformation under Friction. *Acta Mech. Solida Sin.* **2021**, *34*, 977–988. [CrossRef]
19. Krishnasamy, M.; Shinde, J.R.; Mohammad, H.P.; Deepesh, U.; Lenka, T.R. Design and Simulation of Smart Flooring Tiles Using Two-Phased Triangular Bimorph Piezoelectric Energy Harvester. In Proceedings of the 2020 IEEE-HYDCON International Conference on Engineering in the 4th Industrial Revolution, HYDCON 2020, Hyderabad, India, 11–12 September 2020; pp. 19–22. [CrossRef]
20. Yingyong, P.; Thainiramit, P.; Jayasvasti, S.; Thanach-Issarasak, N.; Isarakorn, D. Evaluation of Harvesting Energy from Pedestrians Using Piezoelectric Floor Tile Energy Harvester. *Sens. Actuators A Phys.* **2021**, *331*, 113035. [CrossRef]
21. Panthongsy, P.; Isarakorn, D.; Hamamoto, K.; Janphuang, P. Performance and Behavior Analysis of Piezoelectric Energy Harvesting Floor Tiles. In Proceedings of the 2019 5th International Conference on Engineering, Applied Sciences and Technology, ICEAST 2019, Luang Prabang, Laos, 2–5 July 2019; pp. 1–4. [CrossRef]
22. Duarte, F.; Ferreira, A.; Fael, P. Road Pavement Energy–Harvesting Device to Convert Vehicles' Mechanical Energy into Electrical Energy. *J. Energy Eng.* **2018**, *144*, 04018003. [CrossRef]
23. Puscasu, O.; Counsell, N.; Herfatmanesh, M.R.; Peace, R.; Patsavellas, J.; Day, R. Powering Lights with Piezoelectric Energy-Harvesting Floors. *Energy Technol.* **2018**, *6*, 906–916. [CrossRef]
24. Kim, K.B.; Cho, J.Y.; Hamid, J.; Ahn, J.H.; Do Hong, S.; Woo, S.B.; Sung, T.H. Optimized Composite Piezoelectric Energy Harvesting Floor Tile for Smart Home Energy Management. *Energy Convers. Manag.* **2018**, *171*, 31–37. [CrossRef]
25. Zhang, Y.; Luo, A.; Wang, Y.; Dai, X.; Lu, Y.; Wang, F. Rotational Electromagnetic Energy Harvester for Human Motion Application at Low Frequency. *Appl. Phys. Lett.* **2020**, *116*, 053902. [CrossRef]
26. Islam, E.; Abdullah, A.M.; Chowdhury, A.R.; Tasnim, F.; Olivares, C.; Lozano, K.; Uddin, M.J. Hybrid Triboelectric-Electromagnetic Energy Tile for Biomechanical Energy Scavenging. *Nano Energy* **2020**, *77*, 105250. [CrossRef]
27. Balato, M.; Costanzo, L.; Lo Schiavo, A.; Vitelli, M. Optimization of Both Perturb & Observe and Open Circuit Voltage MPPT Techniques for Resonant Piezoelectric Vibration Harvesters Feeding Bridge Rectifiers. *Sens. Actuators A Phys.* **2018**, *278*, 85–97. [CrossRef]
28. Ajitsaria, J.; Choe, S.Y.; Shen, D.; Kim, D.J. Modeling and Analysis of a Bimorph Piezoelectric Cantilever Beam for Voltage Generation. *Smart Mater. Struct.* **2007**, *16*, 447–454. [CrossRef]
29. Lefeuvre, E.; Audigier, D.; Richard, C.; Guyomar, D. Buck-Boost Converter for Sensorless Power Optimization of Piezoelectric Energy Harvester. *IEEE Trans. Power Electron.* **2007**, *22*, 2018–2025. [CrossRef]
30. Mitcheson, P.D.; Toh, T.T.; Wong, K.H.; Burrow, S.G.; Holmes, A.S. Tuning the Resonant Frequency and Damping of an Electromagnetic Energy Harvester Using Power Electronics. *IEEE Trans. Circuits Syst. II Express Briefs* **2011**, *58*, 792–796. [CrossRef]
31. Cai, Q.L.; Zhu, S. Enhancing the Performance of Electromagnetic Damper Cum Energy Harvester Using Microcontroller: Concept and Experiment Validation. *Mech. Syst. Signal Process.* **2019**, *134*, 106339. [CrossRef]
32. Cai, Q.; Hua, Y.; Zhu, S.; Zhang, X.; Zuo, H. Bistable Energy-Harvesting Track Nonlinear Energy Sink in Offshore Wind Turbines. *Mech. Syst. Signal Process.* **2024**, *215*, 111407. [CrossRef]
33. Williams, C.B.; Yates, R.B. Analysis of a Micro-Electric Generator for Microsystems. *Sens. Actuators A Phys.* **1996**, *52*, 8–11. [CrossRef]
34. Boisseau, S.; Despesse, G.; Ricart, T.; Defay, E.; Sylvestre, A. Cantilever-Based Electret Energy Harvesters. *Smart Mater. Struct.* **2011**, *20*, 105013. [CrossRef]
35. Tian, W.; Ling, Z.; Yu, W.; Shi, J. A Review of MEMS Scale Piezoelectric Energy Harvester. *Appl. Sci.* **2018**, *8*, 645. [CrossRef]
36. Durgadevi, S.; Anbazhagan, R.; Harini, R.; Vimonisha, A. A Review of Performance Optimization of Footstep Energy Harvester. In Proceedings of the International Conference on Communication, Computing and Internet of Things, IC3IoT 2022, Chennai, India, 10–11 March 2022; pp. 1–5. [CrossRef]
37. Wickenheiser, A.M.; Reissman, T.; Wu, W.J.; Garcia, E. Modeling the Effects of Electromechanical Coupling on Energy Storage through Piezoelectric Energy Harvesting. *IEEE/ASME Trans. Mechatron.* **2010**, *15*, 400–411. [CrossRef]
38. Wei, C.; Jing, X. A Comprehensive Review on Vibration Energy Harvesting: Modelling and Realization. *Renew. Sustain. Energy Rev.* **2017**, *74*, 1–18. [CrossRef]

39. Khojet, S.; Khil, E.; Youssef, A.B.; Slama Belkhodja, I. Single Phase PWM Rectifier Sensor Fault Tolerant Control Based on Residual Generation. *J. Electr. Syst.* **2018**, *14*, 190–204.
40. Rashid, M.H. *Power Electronics Handbook*; Butterworth-Heinemann: Oxford, UK, 2017.
41. Mitra, A.; Chowdhuri, S. Analysis of Single Phase PWM Rectifier for Different Applications. *J. Inst. Eng. India Ser. B* **2017**, *98*, 161–169. [CrossRef]
42. Huang, X.; Chang, D.; Ling, C.; Zheng, T.Q. Research on Single-Phase PWM Converter with Reverse Conducting IGBT Based on Loss Threshold Desaturation Control. *Energies* **2017**, *10*, 1845. [CrossRef]
43. Tan, R.H.G.; Er, C.K.; Solanki, S.G. Modeling of Photovoltaic MPPT Lead Acid Battery Charge Controller for Standalone System Applications. In Proceedings of the E3S Web of Conferences, Lisboa, Portugal, 19–21 October 2020; Volume 182, pp. 1–7. [CrossRef]
44. Tadmor, E.B.; Kósa, G. Electromechanical Coupling Correction for Piezoelectric Layered Beams. *J. Microelectromechanical Syst.* **2003**, *12*, 899–906. [CrossRef]
45. Morbiato, T.; Borri, C.; Vitaliani, R. Wind Energy Harvesting from Transport Systems: A Resource Estimation Assessment. *Appl. Energy* **2014**, *133*, 152–168. [CrossRef]

Disclaimer/Publisher's Note: The statements, opinions and data contained in all publications are solely those of the individual author(s) and contributor(s) and not of MDPI and/or the editor(s). MDPI and/or the editor(s) disclaim responsibility for any injury to people or property resulting from any ideas, methods, instructions or products referred to in the content.